A novel Graphene/Heusler Alloy Heterostructure for Advanced Spintronics

Songtian Li[a], Pavel B. Sorokin[b], Shiro Entani[a], Kenta Amemiya[c], Yuya Sakuraba[d], and Seiji Sakai[a]

[a]*National Institutes for Quantum and Radiological Science and Technology, 1233 Watanuki, Takasaki 370-1292, Japan*
[b]*National University of Science and Technology, 4 Leninskiy prospect, Moscow 119049, Russian Federation*
[c]*High Energy Accelerator Research Organization, 1-1 Oho, Tsukuba 305-0801, Japan*
[d]*National Institute of Materials Science, 1-2-1 Sengen, Tsukuba 305-0047, Japan*

Keywords: spintronics, graphene, Heusler alloy, XMCD

The graphene-based spintronic devices are receiving an intensive interest due to the great potential for next-generation ultrafast and lower-power-consumption memory and logic technology. [1, 2] Nevertheless, the performance in the developed graphene-based spintronic device up to dates are found too poor to satisfy the requirement for real device application. The low spin polarization of the ferromagnets involved in the reported graphene-based spintronic devices is thought to be one of the main reasons corresponds to the poor performance. Thus, the adoption of ferromagnets with high spin polarization into graphene-based spintronic devices are crucial to improve the performance. This report presents our recent efforts on the successfully fabrication of a novel heterostructure consisting of CVD-grown single-layer graphene on half-metallic full Heusler alloy $Co_2Fe(Ge_{0.5}Ga_{0.5})$ (CFGG, hereafter) ferromagnet with high spin polarization.[3] The quality and interfacial electronic and magnetic properties were investigated in order to evaluate the feasibility by using this new heterostructure for advanced spintronic device applications.

The quality of the graphene grown on CFGG was characterized by Raman spectroscopy as shown in Fig.1(a). The small intensity of the defect-induced D band compared to the G band suggests a high crystal quality of graphene formed on CFGG. Fig.1(b) shows the x-ray absorption spectroscopy XAS spectra at the C *K*-edge obtained in the partial-electron-yield (PEY) mode at the x-ray incident angle α of 30° and 90° with respect to the sample surface, respectively. We observed a sharp peak (285 eV) due to the π* resonance of graphene, as well as the peak (290~300 eV) due to the σ* resonance. The sharpness of the π* resonance peak

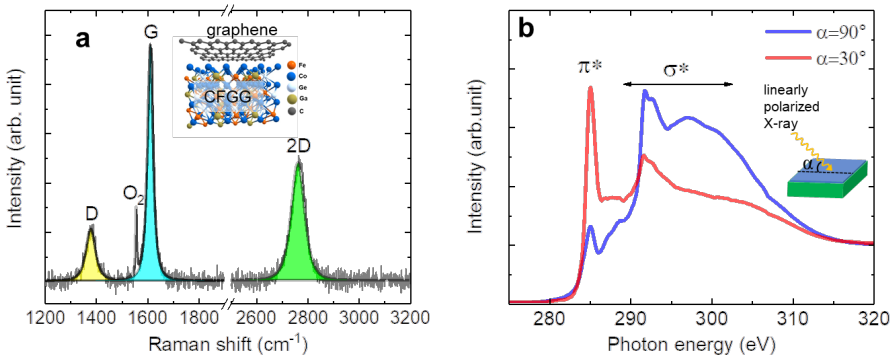

Figure 1. a) Raman spectrum of graphene/CFGG heterostructure. b) C *K*-edge XAS spectra. The sharp peak at 1557 cm^{-1} of (a) is attributed to O_2 in ambient air. Inset of (a) is a sketch of the graphene/CFGG heterostructure.

in the graphene/CFGG heterostructure is markedly different from that in the heterostructures of graphene and other ferromagnets, where a significant splitting and broadening of the π* resonance peak was reported in association with the orbital hybridization between graphene and ferromagnets. This result indicates CFGG does not cause a severe degradation in the electronic properties of graphene.

The magnetic properties at the interface region of the CFGG thin film in the graphene/CFGG heterostructure were explored by depth-resolved (DR) x-ray magnetic circular dichroism (XMCD) spectroscopy. Figs 2(a) and (b) compare the XAS and XMCD spectra at the Co and Fe $L_{2,3}$-edges obtained in the bulk-sensitive total-electron-yield (TEY) mode and the DR-PEY mode under the surface-sensitive condition with mean probing depth $\lambda_p \sim 4$ Å, which corresponds to the outermost surface located at the graphene/CFGG interface. The spectroscopic features of the TEY and DR-PEY XAS spectrum are compatible with each other, which indicates a carbide free graphene/CFGG interface. The evaluated total magnetic moments (m_{total}) per atom and their spin and orbital components (m_{spin} and m_{orb}, respectively) evaluated from the TEY XMCD spectrum and the series of the DR-PEY XMCD spectra obtained at different emission angles are summarized in Figs. 2(c) and (d). It is found that, only a slight decrease of magnetic moment was found at the interface comparing to that of the bulk region. The preservation of the large magnetic moment throughout the interface region is in sharply contrast to the significant reduction as reported for other heterostructure such as graphene/Fe.[4]

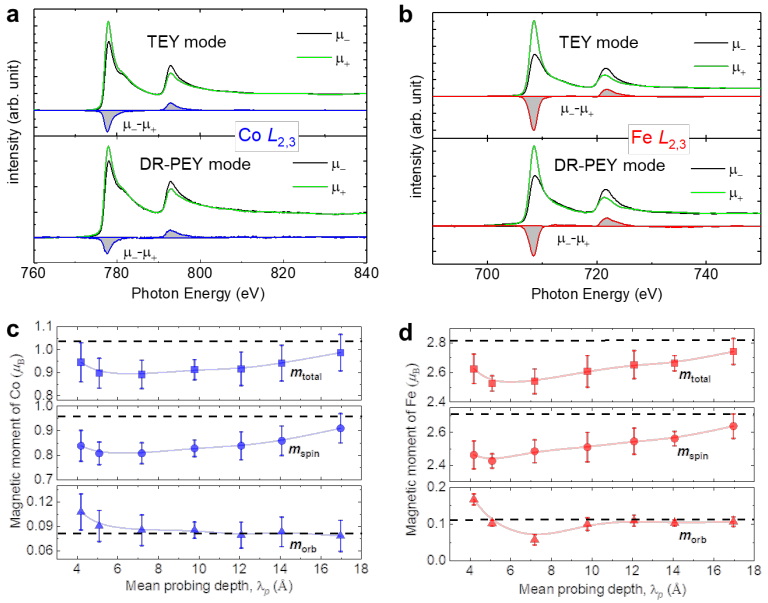

Figure 2. (a, b) Comparison of XAS and XMCD spectra of SLG/CFGG heterostructure at Co and Fe $L_{2,3}$-edges obtained in TEY and DR-PEY modes. (c, d) Plots for orbital, spin and total magnetic moment of Co, and Fe *vs.* mean probing depth (λ_p). The DR-PEY spectra in (a) and (b) are at $\lambda_p \sim 4$ Å. The dashed lines in (c) and (d) indicate the magnetic moments evaluated from the TEY XMCD spectra.

The unusual preservation of the inherent electronic and magnetic properties at the graphene/CFGG interface indicates a dramatic improvement in the efficiency of spin injection and transport in graphene comparing to other graphene/ferromagnet heterostructures. Our results suggest the newly developed graphene/CFGG heterostructure can be a very potential building block for high-performance graphene spintronic device application.

REFERENCES

1. W. Han *et. al*., *Nat. Nanotechnol.* ***9***, 794 (2014). 2. E. D. Cobas *et. al*., *ACS Nano* **10**, 10357 (2016).

3. S. Li *et. al*., *Adv. Mater*. Adv. Mater. **32**, 1905734 (2020). 4. W.Q. Liu *et. al*., *Sci. Rep*. **5**, 11911 (2015).

Role of Ion Beams in $SrTiO_3$ and their Characterizations by Synchrotron Based Techniques

K. Asokan[a], Vishnu Kumar[b], Anuradha Bhogra[a] C.L. Dong[c], C.L. Chen[d], S. Annapoorni[b],

[a]*Inter University Accelerator Centre, Aruna Asaft Ali Marg, New Delhi-110067 India*
[b]*Department of Physics and Astrophysics, University of Delhi, Delhi 110 0 07 India*
[c]*Department of Physics, Tamkang University, Tamsui 25137, Taiwan*
[d]*National Synchrotron Radiation Research Center, Hsinchu 30076, Taiwan*

Keywords: Ion beam interactions, X-ray Absorption Spectroscopy, Oxides, $SrTiO_3$, Photoluminescence

The quantum materials encompass various materials and phenomena leading to new dimensions. Understanding the role of ion beams in these materials like $SrTiO_3$ (STO) using synchrotron-based characterization like x-ray diffraction (XRD), Photoluminescence (PL), and X-ray Absorption Near-Edge Structure (XANES) spectroscopic techniques may lead to novel properties and applications [1-3]. We report the evolution of optical intense blue-green emission in 100 keV nitrogen (N) ion implanted STO thin films. The XRD pattern shows a change in reflections at lower N ion fluences and the amorphization of the films at higher fluencies. A disordered phase induced by implantation in the STO films leads to an intense blue-green emission due to oxygen (O) vacancies and N (2*p*) bound states. A schematic diagram of energy levels has been proposed to explain the origin of PL emission. The XANES spectra at Ti *K* edge reflect a change in the valency of Ti ions and the local atomic structure of ordered and disordered phases of STO with an increase in N ion fluence. The splitting of peak assigned to e_g orbitals, and change in ratio $d_z^2/d_{x^2-y^2}$ observed in the Ti *L*- and O *K*-edge spectra, confirm a distortion in TiO_6 octahedral structure and modifications in O 2*p*-Ti 3*d* hybridization states. The synchrotron-based techniques reveal that N ion implanted STO can be a good photoluminescent material exhibiting a variety of emissions through bound states of O vacancies and implanted N ions. Similar investigations were also carried out to understand the changes in the electrical and thermoelectrical properties of N ion implanted STO[3].

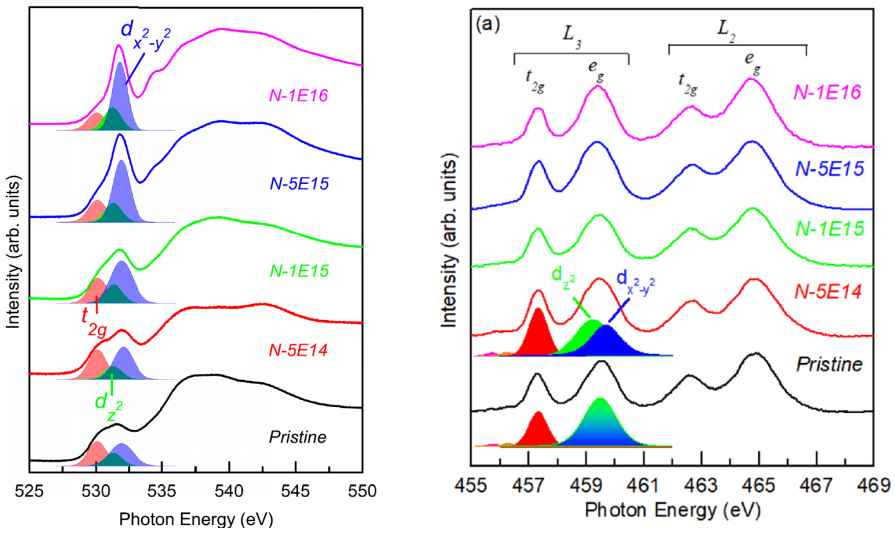

FIGURE 1. The normalized XANES spectra at (i) O K-edge and (ii) Ti L-edges of N ion implanted STO thin films. Note the evolution of spectral features with N ion implantations [1].

REFERENCES

1. V. Kumar, et al Physical Rev B Kumar, V., Bhogra, A., Bala, M., Haw, S.C., Chen, C.L., Dong, C.L., Asokan, K., Annapoorni, S. *Physical Review B,* **103** (2), art. no. 024104.(2021).
2. Kumar, V., Bhogra, A., Bala, M., Kuo, H.-W., Chen, C.-L., Dong, C.-L., Kandasami, A., Subramanian, A. *Scripta Materialia*, **195**, art. no. 113725 (2021).
3. Bhogra, A., *et al, Scientific Reports,* **9** (1), art. no. 14486 (2019) .

Marvel CPL, CPLE, and ECD Spectroscopy to Study the Origin of CD- and CPL-sign Inversion of *D*-/*L*-Camphor and Colloidal π-Conjugated Polymers

Michiya Fujiki[a]

[a]Devision of Materials Science, Graduate School of Science and Technology,
Nara Institute of Science and Technology, 8916-5 Takayama, Ikoma, Nara 630-0192, Japan

Keywords: circularly polarized luminescence, circular dichroims, circularly polarized luminescence excitation, camphor, photoexcited state, ground state, chirality, polymer, colloid, anti-Kasha's rule

Kasha's rule is one of the most crucial guiding principles of how photoexcited luminophores in S_n (n = 1, 2, 3...) states relax radiatively and non-radiatively to the ground state (S_0). However, an open question remains yet whether the Kasha's rule is always valid for chiral luminophores. Early works of *D*- and *L*-camphors reported bisignate dual CPL characteristics at 370 nm (minor) and 450 nm (major) [1–3]. The sign of the 450-nm CPL band is opposite to that of the first Cotton CD signal at 290 nm. The origin of anomaly, so-called anti-Kasha's rule, is obscure. Nowadays, electronic circular dichroism (ECD) spectroscopy is widely utilized to characterize the S_0-state chirality of chromophores. On the other hand, circularly polarized luminescence (CPL) spectroscopy allows for direct detection S_1-state chirality of luminophores. Moreover, CPL excitation (CPLE) spectroscopy teaches directly the origin of CPL band by monitoring at a specific (+)- and (–)-sign CPL band because CPLE is an electronic band selective spectroscopy.

Herein, we applied these CPL, CPLE, and CD spectroscopy to account for the dual CPL band associated with the sign inversion between CD and CPL bands of *D*- (or *L*-) camphor [4]. With help of DFT/TD-DFT calculations, we concluded that *D*- (or *L*-) camphor adopts a planar ketone form with (+)-sign CD band at ~300 nm in the S_0 state, while camphor adopts a bent ketone form associated with (–)-sign CD band at ~350 nm in the S_1 state (Fig. 1). The former is thermodynamically stable and the latter is metastable by 12 Kcal mol^{-1}. The bent and planar ketone forms in the photoexcited *D*-camphor are responsible for the bisignate dual CPL band (Fig. 2b), while the planar form, dominant species in the S_0 state, reveals the monosignate CD band (Fig. 2a) [4]. The corresponding CPLE spectra monitored at 370 nm and 480 nm (Fig. 2c and 2d) agree well with this conclusion.

Likewise, dual CPL and couple-like CD band profiles from colloidal π-conjugated polymer (**PF8T2**) generated with helical polysilanes (**PSi-*S*** and **PSi-*R***) teach us that the colloidal **PF8T2** in the photoexcited state does not obey the convesional Kasha's rule, as shown in Fig. 3a and 3b [4].

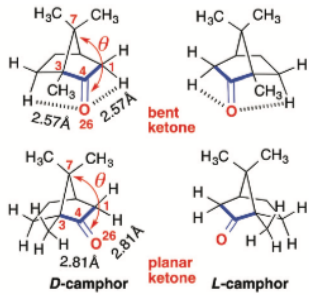

FIGURE 1. (Bottom) Planar ketone forms in the ground states and (top) bent ketone forms in the photoexcited states of *D*- and *L*-camphors, that are optimized by DFT (B3LYP, aug-ccpvDZ basis set) [4].

Our results suggest that the photoexcited chirality significantly differs from the ground state chirality owing to reorganization process of luminophores at the S_n states, that often unveils spectroscopically as (i) Stokes shift, (ii) an apparent inversion in chiroptical signs between CD at the first Cotton band and CPL

band, and (iii) incomplete couplet-like dual CPL bands associated with couplet-like dual CD bands [5,6]. We assume that, in the realms of photophysics and photochemistry, anti-Kasha's rule is a common, universal concept rathar than the convesional Kasha's rule [7–10].

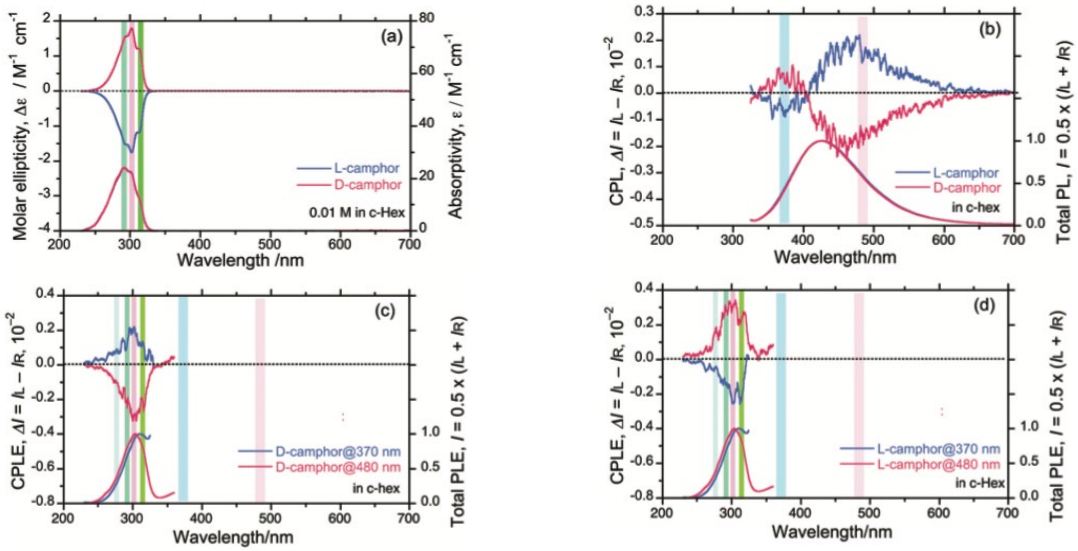

FIGURE 2. Vibronic CD spectra (a), structureless CPL spectra (b), and vibronic CPLE spectra monitored at 370 nm and 480 nm (c) and (d), respectively, of *D*- and *L*-camphors in dilute cyclohexane [4].

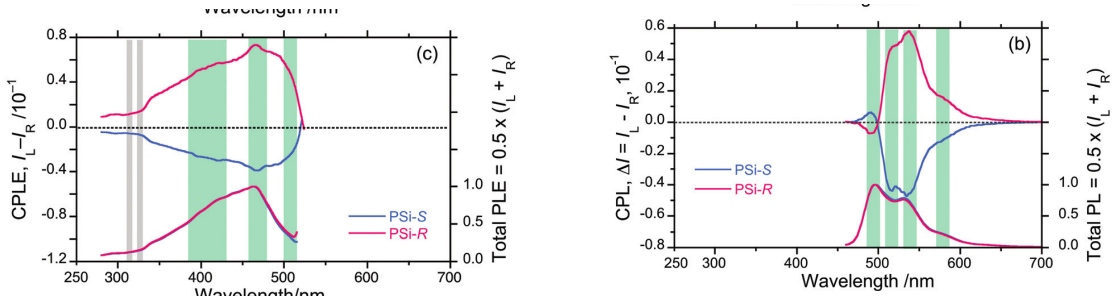

FIGURE 3. Chemical structures of optically active π-conjugated polymer (**PF8T2**) endowed with helical polysilanes (**PSi-*S*** and **PSi-*R***). (a) Couplet-like dual CD bands in the range of 350 nm and 550 nm and (b) couplet-like dual CPL bands in the range of 450 nm and 650 nm in a mixture of chloroform-methanol [4].

REFERENCES

1. H.P.J.M. Dekkers and L.E. Closs, *J. Am. Chem. Soc*., **1976**, *98*, 2210–2219.
2. P. H. Schippers, J.P.M. van der Ploeg, and H.P.J.M. Dekkers, *J. Am. Chem. Soc.*, **1983**, *105*, 84–89.
3. G. Longhi, E. Castigilioni, S. Abbate, F. Lebon, and D.A. Lightner, *Chirality*, **2013**, *25*, 589–599.
4. S.T. Duong and M. Fujiki, *Polym. Chem*., **2017**, *8*, 4673–4679.
5. M. Fujiki, *Symmetry*, **2021**, *13*, 199.
6. L. Wang, L. Yin, W. Zhang, X. Zhu, and M. Fujiki, *J. Am. Chem. Soc.,* **2017**, *139,* 13218–13226.
7. J. Gierschner, S. K. Behera, and S. Y. Park, *Angew. Chem. Int. Ed.* 2020 (doi.org/10.1002/anie.202009789).
8. M. Röhrs and D. Escudero, *J. Phys. Chem. Lett.*, **2019**, *10*, 5798–5804.
9. J.C. DelValle and J. Catalán, *Phys. Chem. Chem. Phys.*, **2019**, *21*, 10061–10069.
10. A.P. Demchenko, V.I. Tomin, and P.T. Chou, *Chem. Rev*., **2017**, *117*, 13353–13381.

Biomolecules Derived-Marine Ecosystems as Attractive Targets for SRCD Applications

Mohamed I. A. Ibrahim[a], Eman H. Zaghloul[b], Ghada E. Hegazy[b], Abeer A. M. El-Sayed[a], Madelyn Moawad[a], Mohamed Saleh Amer[b]

[a]*Laboratory of Marine Chemistry, Marine Environment Division, National Institute of Oceanography & Fisheries, NIOF, Egypt*
[b] *Laboratory of Microbiology, Marine Environment Division, National Institute of Oceanography & Fisheries, NIOF, Egypt*

Keywords: Marine ecosystems, Exopolysaccharides, Carotenoids, Bioactive molecules

Marine ecosystems are aquatic environments of high salinity levels with characteristics physical and biological features [1]. They have been regarded as promising sources for isolation of new microorganisms (fungi, bacteria and actinomycetes) which are powerful producers of bioactive natural products *e.g* biodegradable polyesters, exopolysaccharides, carotenoids, *etc*. [2-4]. For example, the fungal exopolysaccharide produced by *Aspergillus terreus* (isolated from marine sediment) has been reported as anticoagulant and possesses cytotoxic activities against breast cancer and human skin fibroblast cell lines (IC_{50} > 100 mg/mL and IC_{50} ~ 47 mg/mL), respectively [4]. In addition, the C_{50} carotenoid bacterioruberin was found to be the predominant compound produced by *Natrialba* sp. M6 of marine origin, which demonstrated potent anticancer and antiviral activities [2]. Although numerous studies reported promising applications of several biomolecules derived from natural origin, rare studies went deep for their structural elucidation using Synchrotron-Radiation Circular-Dichroism spectroscopy (SRCD) [3, 5, 6]. In this context, there is a necessity of using SRCD for providing more detailed information about the secondary structure and the contents of α-helix and β-strand segments with high accuracy. Then, combining SRCD data with bioinformatics can predict the tertiary-structure model of a protein which may facilitate understanding its biological mechanism of action [7].

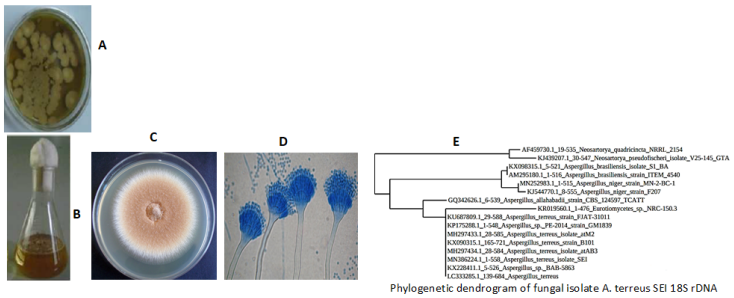

FIGURE 1. Isolation, production and purification of exopolysaccharide produced from marine-derived *Aspergillus terreus* SEI with prominent biological activities.

REFERENCES

1. K. Smyth and M. Elliott, in *Stressors in the Marine Environment*, eds. S. Martin and W. Nia, Open University Press Editors: , 2016, DOI: 10.1093/acprof:oso/9780198718826.003.0009, ch. 9.
2. G. E. Hegazy, M. M. Abu-Serie, G. M. Abo-Elela, H. Ghozlan, S. A. Sabry, N. A. Soliman and Y. R. Abdel-Fattah, *Sci. Rep.*, 2020. **10**(1): p. 5986.
3. J. V. Pham, M. A. Yilma, A. Feliz, M. T. Majid, N. Maffetone, J. R. Walker, E. Kim, H. J. Cho, J. M. Reynolds, M. C. Song, S. R. Park and Y. J. Yoon, 2019. **10**(1404).
4. M. Saleh Amer, E. H. Zaghloul and M. I. A. Ibrahim, *Egypt. J. Aquat. Res.*, 2020. **46**(4): p. 363-369.
5. A. L. Demain, E. Vandamme, J. Collins and Z. BuchhoI, *History of industrial biotechnology, In: Industrial Biotechnology: Microorganisms*, Wiley-VCH, Weinheim, 2017.
6. K. Rogers, *Biomolecule*, 2020: p. Encyclopedia Britannica, https://www.britannica.com/science/biomolecule.
7. Matsuo and K. Gekko, *In: Lipid-Protein Interactions*, Methods in Molecular Biology, vol 2003. Humana, New York, NY, 2019.

Equilibrium and Ultrafast Response of Topological Matter to Optical Excitation

Jaime Sánchez-Barriga[a]

[a] *Helmholtz-Zentrum Berlin für Materialien und Energie, Elektronenspeicherring BESSY II, Albert-Einstein-Str. 15, 12489 Berlin, Germany*

Keywords: Topological materials, topological surface states, topological quantum phase transitions, spin- and angle-resolved photoemission, time-resolved photoemission, synchrotron radiation, ultrafast optical excitation.

In this talk, I will provide an overview of my research activity on spin-based phenomena in topological materials primarily using time-, spin- and angle-resolved photoemission as well as synchrotron-radiation methods. In the first part of the talk, I will concentrate on the spin-dependent properties of topological surface states (TSSs) in equilibrium by highlighting previous and recent results obtained using synchrotron-based photoemission at the RGBL-2 end-station permanently installed at the U125/2 undulator beamline of the synchrotron source BESSY-II in Berlin. This includes the first commissioning results concerning the spin texture manipulation of emitted photoelectrons from TSSs, the direct observation of magnetic and non-magnetic gaps at the Dirac point of TSSs and hedgehog spin textures, as well as the realization of topological quantum-phase transitions between topological crystalline insulators and strong topological insulators.

In the second part of the talk, I will focus on dynamical aspects such as observation of ultrafast spin-polarized electrical currents in energy-momentum space, the emergence of anisotropic coherent-phonon oscillations on topological insulator surfaces or the electron relaxation dynamics near the critical point of a trivial to topological quantum-phase transition. Finally, I will discuss the impact of ultrafast carrier transport on the dynamics of TSSs following laser excitation, and describe how the complex and alternating transient spin textures observed above the Fermi level on sub-picosecond time scales affect the ultrafast channels of charge and energy transfer that are relevant for the relaxation of carriers.

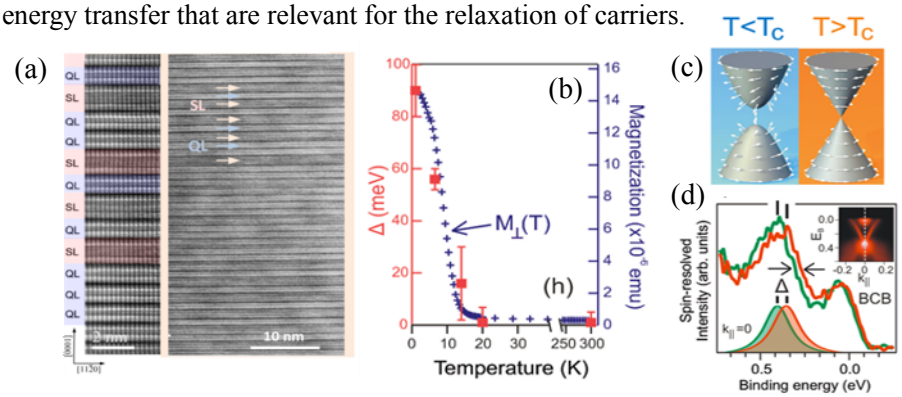

FIGURE 1. Example of a large magnetic gap at the Dirac point in Mn-doped Bi_2Te_3. The system exhibits (a) a self-organized alternating sequence of $MnBi_2Te_4$ septuple and Bi_2Te_3 quintuple layers, (b) an out-of-plane magnetic anisotropy which correlates with a band gap opening at the Dirac point of the topological surface state only below the Curie temperature T_c, and (c),(d) a ferromagnetic out-of-plane spin texture which can be resolved using spin- and angle-resolved photoemission [3].

REFERENCES

1. O. J. Clark, F. Freyse, I. Aguilera, A. Ionov, S. Bohzko, L. V. Yashina and J. Sánchez-Barriga, *submitted* (2021)
2. A. Varykhalov, F. Freyse, I. Aguilera, M. Krivenkov, D. Marchenko, G. Bihlmayer, S. Blügel, O. Rader and J. Sánchez-Barriga, *Physical Review Research* **2**, 013343 (2020)
3. E. Rienks*, S. Wimmer*, J. Sánchez-Barriga*, O. Caha*, P. S. Mandal, J. Ruzicka, A. Ney, H. Steiner, V. V. Volobuev, H. Groiss, M. Albu, G. Kothleitner, J. Michalicka, S. Khan, J. Minár et al., *Nature* **576**, 423 (2019).
4. P. S. Mandal, G. Springholz, V.V. Volobuev, O. Caha, A. Varykhalov, E. Golias, G. Bauer, O. Rader, and J. Sánchez-Barriga , *Nature Communications* **8**, 968 (2017)
5. J. Sánchez-Barriga *et al.*, M. Battiato, M. Krivenkov, E. Golias, A. Varykhalov, A. Romualdi, L. V. Yashina, J. Minár, O. Kornilov, H. Ebert, K. Held, J. Braun, *Physical Review B* **95**, 125405 (2017)
6. J. Sánchez-Barriga, A. Varykhalov, G. Springholz, H. Steiner,R. Kirchschlager, G. Bauer, O. Caha, E. Schierle, E. Weschke, A. A. Ünal, S. Valencia, M. Dunst, J. Braun, H. Ebert, J. Minár et al., *Nature Communications* 7, 10559 (2016)

Electronic correlations of CeSb through the devil's staircase transition

Kenta Kuroda

ISSP, The University of Tokyo, Japan

Keywords: strong correlation, transition, magnetism, photoemission, laser

Solids with competing interactions often undergo complex phase transitions with a variety of long-periodic modulations. Among such transition, devil's staircase is the most complex phenomenon, and for it, CeSb is the most famous material, where a number of the distinct phases with long-periodic antiferromagnetostructures sequentially appear below the Néel temperature [1]. An evolution of the low-energy electronic structures and underlying electronic correlations going through the devil's staircase is of special interest to understand its mechanism, which has, however, been elusive despite 40 years of intense research.

In my presentation, I will talk about our recent investigations of the electronic properties undergoing the devil's staircase by using laser-based angle-resolved photoemission spectroscopy. So far, the paramagnetic electronic structure with the semimetallic feature was well documented in detail: two hole pockets of Sb 5*p* at Γ point and an electron pocket of Ce 5*d* at X point [2]. The high-energy resolution and bulk-sensitivity achieved by utilizing our low-energy laser source ($h\nu = 7$ eV) now reveals the significant reconstruction of these itinerant bands and the many-body interactions, which have so far evaded from the experimental detection. The reconstruction of conducting bands to the 4*f* order is sensitively changed at each distinct transition of the devil's staircase, and it exposes the strong electronic anisotropy across T_N. The change of the spectral property against magnetic reconstructions is surprisingly dramatic [3]. Moreover, we discovered a new type of electron-boson coupling between the mobile electrons and crystal-electric-field excitations of the 4*f*-orbitals, which renormalizes the Sb 5*p* band prominently, yielding a remarkable kink at very low-energy. This coupling strength of the many body state is exceedingly strong and exposes anomalously enhancement during the devil's staircase transition [4].

REFERENCES

1. J. Rossat-Mignod, Journal of Magnetism and Magnetic Materials **52**, 111 (1985).
2. K. Kuroda *et al*., Physical Review Letters **120**, 086402 (2018).
3. K. Kuroda *et al*., Nature Communications **11**, 2888 (2020).
4. Y. Arai, K. Kuroda *et al*., submitted.

Doping Dependence of The Electronic Structure in Triple-layer Cuprate Bi2223

S. Ideta[a,b], K. Tanaka[a,b], T. Yoshdia[c], S. Adachi[d], S. Yamaguchi[d], N. Sasaki[d], T. Watanabe[d], T. Noji[e], S. Ishida[f], S. Uchida[f,h], and A. Fujimori[g,h]

[a] *Institute for Molecular Science, UVSOR-III Synchrotron Okazaki, 444-8585, Japan*
[b] *SOKENDAI (The Graduate University for Advanced Studies), Okazaki 444-8585, Japan*
[c] *Department of Human and Environmental studies, Kyoto University, Sakyo-ku, Kyoto 606-8501, Japan*
[d] *Graduate School of Science and Technology, Hirosaki University, Hirosaki, Aomori 036-8561, Japan*
[e] *Department of Applied Physics, Graduate School of Engineering, Tohoku University, Sendai, Miyagi 980-8579, Japan*
[f] *National Institute of Advanced Industrial Science and Technology, Tsukuba, Ibaraki 305-8568, Japan*
[g] *Department of Applied Physics, Waseda Unversity, Shinjuku-ku, Tokyo 169-8555, Japan*
[h] *Department of Physics, University of Tokyo, Bunkyo-ku, Tokyo 113-0033, Japan*

Keywords: Superconductivity, Cuprate, ARPES, Electronic structure.

The energy gap seen in the superconducting (SC) and normal states has been believed to be an important piece of evidence for the mechanism of high SC transition temperature in cuprate superconductors. Bi-based high-T_c cuprate superconductors can be classified by the number of the neighboring CuO_2 planes (n): single-layer (n = 1) $Bi_2Sr_2CuO_{4+\delta}$ (Bi2201), double-layer (n = 2) $Bi_2Sr_2CaCu_2O_{8+\delta}$ (Bi2212), triple-layer (n = 3) $Bi_2Sr_2Ca_2Cu_3O_{10+\delta}$ (Bi2223). In going from n = 1 to 3, the maximum T_c increases and shows 35 K and 95 K for Bi2201 and Bi2212, respectively. Bi2223 shows 110 K, which is the highest T_c among the Bi family of cuprates [1]. However, the microscopic origin of this trend has not been clear yet.

For optimally doped Bi2223, we have revealed the electronic structure using angle-resolved photoemission spectroscopy (ARPES) [2-5]. However, it has been known that the sample fabrication with different doping is very difficult and the doping dependence of the electronic structure could not be investigated so far. Recently, high quality underdoped and overdoped single crystals of Bi2223 has been successfully synthesized [6,7]. We have performed a high-resolution ARPES study using synchrotron radiation, and revealed the doping dependent electronic structure in Bi2223. In this presentation, we will show the electronic structure of underdoped, optimally doped, and overdoped Bi2223 and discuss the origin of the high T_c in Bi2223.

REFERENCES

1. A. Iyo *et al*., *J. Phys. Soc. Jpn*., **76**, 094711 (2007).
2. S. Ideta et al., *Phys. Rev. Lett.* **104**, 227001 (2010).
3. S. Ideta et al., *Phys. Rev. B* **85**, 104515 (2012).
4. S. Kudo *et al*., Phys. Rev. B **92**, 195135 (2015).
5. S. Ideta *et al*., arXiv:2010.15373.
6. S. Adachi *et al*., *Physics Procedia* **65**, 53-56 (2015).
7. S. Adachi *et al*., *J. Phys. Soc. Jpn*., **84**, 024706 (2015).

Coherent Control of Atoms in the Extreme Ultraviolet and Attosecond Regime by Synchrotron Radiation

Tatsuo Kaneyasu[a]

[a]*SAGA Light Source, Tosu 841-0005, Japan*

Keywords: coherent control, attosecond, tandem undulator.

Quantum manipulation of populations and pathways in matter by light pulses, so-called coherent control, is currently one of the hottest research areas in optical physics and photochemistry. In the last two decades, coherent control of a quantum system has been extensively studied using optical lasers which provide phase-locked sequential pulses. Moreover recent advent of the high harmonic laser source and seeded free electron lasers (FELs) has enabled the coherent control at extreme ultraviolet (XUV) regions. We report on a new route to coherent control in the XUV and attosecond regime. Our method is based on the potential use of undulator radiation as longitudinally coherent wave packets, which has been hidden in the incoherent nature of the radiation pulse.

The experiments were carried out at the 750-MeV UVSOR-III storage ring. We used the pairs of 10-cycle radiation wave packets with attosecond-controlled spacing emitted from the tandem undulator consisted of twin APPLE-II type devices [Fig. 1a]. Based on the wave packet interferometry scheme, we succeeded in controlling the population [1] and orbital alignment [2] in photoexcitation of helium atoms in the XUV region by tuning the time delay between the two wave packets at the attosecond level [see Fig 1b]. Since our technique uses a synchrotron light source, it is extendable as far as hard x-ray. This new capability of synchrotron light sources will open up the possibilities of probing and controlling ultrafast phenomena [3] in a wide range of atomic and molecular processes as well as in a variety of materials.

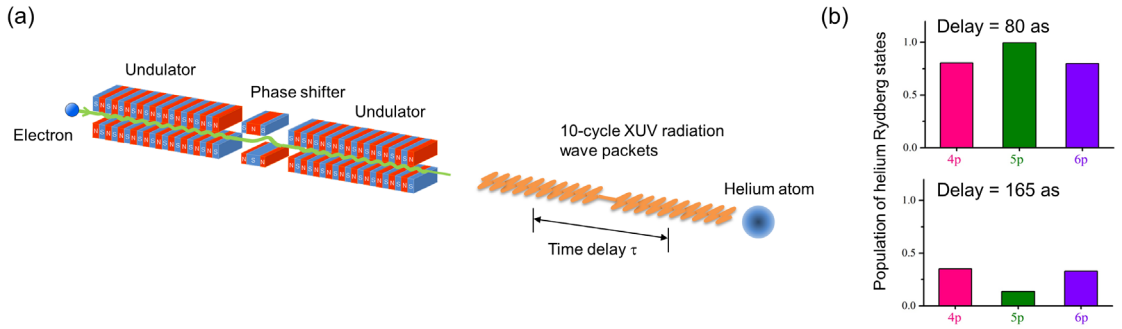

FIGURE 1. (a) Experimental scheme for the population control. The relativistic electron emits a pair of 10-cycle wave packets. (b) The population of excited state is controlled by tuning the time delay between the wave packets at the attosecond level.

REFERENCES

1. Y. Hikosaka et al., *Nat. Commun*. **10**, 4988 (2019).
2. T. Kaneyasu et al., *Phys. Rev. Lett.* **123**, 233401 (2019).
3. T. Kaneyasu et al., *Phys. Rev. Lett.* in press.

An Application of Vacuum Ultraviolet Circular Dichroism Spectroscopy to Radiation Biology: Secondary Structural Analyses of Histone Proteins

Yudai Izumi

Institute for Quantum Life Science, National Institutes for Quantum and Radiological Science and Technology (QST), 2-4 Shirakata, Tokai-mura, Naka-gun, Ibaraki 319-1106, Japan

Keywords: DNA damage repair, DNA double-strand break, post-translational modification, chromatin

1. Introduction

DNA wraps around core histones in eukaryotic nuclei. The core histone is an octamer of histone proteins; two H2A-H2B dimers and an H3-H4 tetramer. Histone proteins have been shown to play a significant role in DNA damage responses (DDRs), such as DNA damage repair. It is assumed that DNA repair processes involve drastic alterations in structure of chromatin (a complex of DNA, histones, and other proteins) to make DNA repair proteins more accessible to damaged sites and such structural changes basically occur via post-translational modifications of histones. However, structural changes in chromatin and histones induced by DNA lesions are scarcely reported. Recently, we observed that secondary structure alterations of H3-H4 are induced by X-ray irradiation of human cancer cells through vacuum ultraviolet circular dichroism (VUV-CD) spectroscopy [1]. We also found that secondary structure contents of methylated histone H3 differed from those of unmethylated H3 *in vitro* [2–4]. In this talk, I will present these results.

2. Materials and Methods

2.1. VUV-CD measurements of H3-H4

Human cancer cells (HeLa.S-FUCCI cells) were cultured and irradiated with X-ray at a dose of 40 Gy. After irradiation, cells were incubated for 30 min to allow for DDRs. The H3-H4 proteins were extracted from the irradiated cells. For comparison, H3-H4 proteins were also extracted from unirradiated cells. The extracted histones were dissolved in 10 mM Tris-HCl buffer supplemented with 250 mM NaF. VUV-CD spectroscopy was carried out at BL-12 of HiSOR. The contents of α-helices, β-strands, turns, and unordered structures were analyzed using SELCON3 programs.

2.2. VUV-CD measurements of methylated H3

Recombinant histone H3 trimethylated at lysine-4, -9, or -36 residues (H3K4me3, H3K9me3, and H3K36me3, respectively) and unmethylated one were purchased and used without further purification. VUV-CD spectroscopy was carried out at BL-12 of HiSOR. The contents of α-helices, β-strands, turns, and unordered structures were analyzed using SELCON3 programs.

3. Results and Discussion

Figure 1 shows VUV-CD spectra of H3-H4 proteins extracted from the unirradiated and irradiated cells. Both samples showed a positive and two negative peaks around 190 and 210–220 nm, respectively. Apparent differences were not observed in the case of negative peaks, but the CD intensities of the positive peaks were lower for irradiated sample than for unirradiated one. Since CD spectra reflect the contents of secondary structures of proteins, the change in CD spectra in the Fig. 1 shows that the structures of H3-H4 proteins extracted from unirradiated and irradiated cells differed from each other, that is, structural alterations of H3-H4 proteins were induced by irradiating the cells with X-rays. Analyzing the CD spectra, we obtained secondary structure contents (Table 1). The decrement of α-helices and increment of β-strands and unordered structures were induced by X-irradiation to cells. It suggests that some amino acid residues which formed α-helix structures before irradiation would be changed into β-strands or unordered ones during and/or after irradiating cells.

The mechanisms underlying the structural alterations of H3-H4 proteins have been unidentified yet. However, we hypothesized that post-translational (de)modifications of histones induced by DDRs changed histone structures because the (de)modifications would affect interactions between histones and DNA and/or

among histones. To confirm that, as a first step, we compared VUV-CD spectra of H3K4me3, H3K9me3, and H3K36me3, which relate to DDRs, with that of unmethylated H3. As shown in Fig. 2, the CD spectral shapes differed from each other. In particular, H3K9me3 exhibited no positive peak in the measurement region. Comparing to the secondary structure contents (Table 2), trimethylation of lysine-4 and -9 residues decreased α-helix structures, but more drastic change was induced by the latter. In contrast, the α-helix content of H3K36me3 was larger than that of unmethylated H3. Thus, trimethylation of histone H3 proteins induced various types of structural alterations depending on the methylation sites. These results would support our hypothesis, that is, post-translational (de)modifications of histones induced by DDRs changed histone structures in the X-irradiated cells.

4. Summary

We observed the structural alterations of H3-H4 in the X-irradiated cells and those of trimethylated H3 using VUV-CD spectroscopy. It is possible that the structural alterations of H3-H4 in the X-irradiated cells were caused by post-translational modifications induced by DDRs.

Acknowledgment

VUV-CD spectroscopy was carried out with the approval of the Hiroshima Synchrotron Radiation Center of Hiroshima University (proposal numbers: 13-B-18, 14-A-16, 15-A-48, 16AU007, 16BG018, and 18AG021). This work was financially supported by JSPS KAKENHI Grant numbers JP15K16130 and JP17K12825.

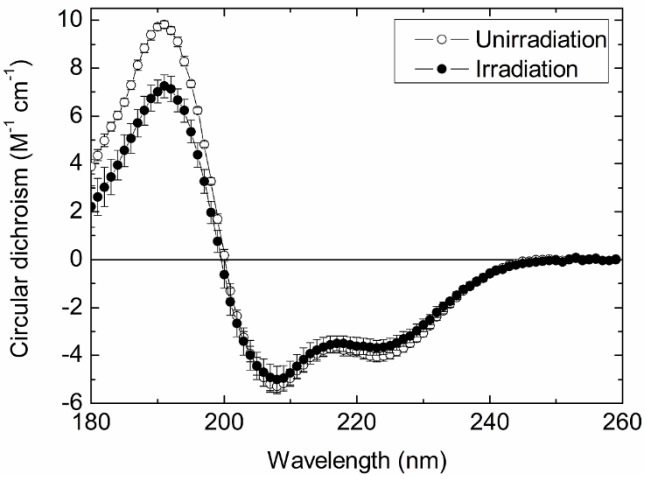

Fig. 1. VUV-CD spectra of H3-H4 extracted from unirradiated and X-irradiated cells.

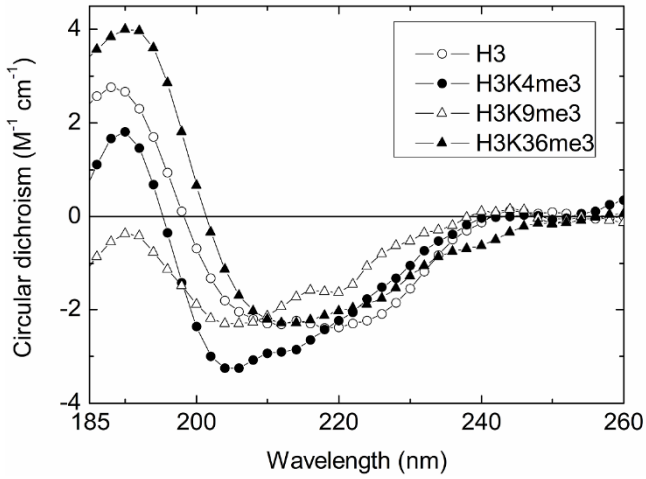

Fig. 2. VUV-CD spectra of unmethylated and trimethylated H3.

TABLE 1. Secondary structure contents of H3-H4 extracted from unirradiated and X-irradiated cells.

Secondary Structures	Unirradiation (%)	Irradiation (%)
α-Helix	61.6±0.6	48.3±0.8
β-Strand	1.9±0.7	8.0±0.3
Turn	18.2±0.6	19.1±0.4
Unordered	17.8±2.5	26.0±1.9

TABLE 2. Secondary structure contents of unmethylated and trimethylated H3.

Secondary Structures	H3 (%)	H3K4me3 (%)	H3K9me3 (%)	H3K36me3 (%)
α-Helix	25.0±1.2	21.8±0.8	13.1±0.8	35.6±1.3
β-Strand	21.3±1.5	25.1±2.0	29.6±1.9	18.7±2.5
Turn	21.1±1.0	21.4±0.7	22.7±1.2	22.3±0.9
Unordered	32.7±1.7	31.7±1.6	36.3±2.4	23.3±2.8

REFERENCES

1. Y. Izumi *et al*., *J. Radiat. Res.* **58**, 59–65 (2017).
2. Y. Izumi *et al*., *J. Radiat. Res.* **59**, 108–115 (2018).
3. Y. Izumi *et al*., *Chirality* **30**, 536–540 (2018).
4. Y. Izumi *et al*., *Molecules* **23**, 2865 (2018).